Elasto-plastic bearing behavior of steel pipes exposed to internal pressure and bending

Peter Schaumann [1], Christian Keindorf [1], Henning Brüggemann [2]

[1] Institute for Steel Construction, University of Hannover, Germany

[2] Dr.-Ing. Veenker Ingenieurgesellschaft mbH, Hannover, Germany

ABSTRACT

Worldwide, actual design standards allow for taking into consideration plastic deformations in order to achieve a higher degree of utilization. In this context maximum plastic strains, which can be allowed for tubular steel pipes exposed to internal pressure and additional loads, are of special interest. In this paper results of investigations on the elasto-plastic bearing behavior of steel pipelines subjected to internal pressure and bending are presented. Four-point bending tests on eight steel pipes on the model scale (D/t = 132) were carried out in order to investigate the buckling behavior in the elasto-plastic range. For the application on buried pipelines Finite-Element (FE)-models were checked by test results. Furthermore an analytical method based on the differential equation for beams with longitudinal tensile force and variable bending stiffness was developed, which is suitable to determine the elasto-plastic bearing capacity for internal pressure and bending. The collapse due to plastic shell buckling is taken into consideration by a limit criterion based on critical strains.

KEY WORDS: pipeline; pressure; bending; elasto-plastic; buckling; strain limit; analytical method

NOMENCLATURE

a	Ovalisation at $\theta = \pi/2$ and $\theta = 3\pi/2$
D	Outer diameter
D_{max}	Maximum measured diameter per pipe cross-section
D_{min}	Minimum measured diameter per pipe cross-section
E	Young's modulus
F	Reaction force
f_o	Initial out-of-roundness
$f_{u,k}$	Characteristic tensile strength
$f_{y,k}$	Characteristic yield strength
I	Moment of inertia of pipe cross-section
M	Bending moment
N	Axial tensile force
P	Internal Pressure
r_m	Average pipe radius
r´	Radius of ovalised pipe
t	Nominal wall thickness
u; u_k	Deformation, imposed deformation
w(x)	Deflection
ε_{el} ; ε_{pl}	Elastic strain; plastic strain
ε_{cr}	Critical strain
$\kappa(x)$	Curvature
ν_{el}	Poisson's ratio in elastic range
σ_L	Longitudinal stress
σ_t ; σ_c	Longitudinal stress (t = tension, c = compression)
σ_Θ	Hoop stress
σ_v	Equivalent stress
σ_y	Yield strength
θ	Circumferential angle

INTRODUCTION

Using an elastic stress analysis for the limit-state design of high-pressure-pipelines is common practice in Germany (DIN EN 1594). Principle of the analysis is to determine the stresses caused by internal pressure and additional loads during erection, operation and service life. To evaluate the biaxial state of stress the available stresses are summarized to the equivalent stress, which must not exceed the yield stress.

The currently valid worldwide standards allow the consideration of plastic deformations in order to reach a higher degree of utilization. In several standards and publications limit states exist for pipelines loaded by combinations of internal pressure and bending. This paper focusses on the question, which maximum plastic strains can be allowed for typical tubular steel under internal pressure and additional loads, bearing in mind the demands for load-capacity, integrity and safety of pipelines.

The aim of the research is to demonstrate the benefits of limit state design for high pressure pipelines based on the consideration of plastic strains and to add experimental and numerical data for the validation. Limit values satisfying the requirements for safety and economy have to be defined.

MODEL SCALE TESTS

To investigate the elasto-plastic bearing behavior of steel pipelines subject to internal pressure and bending a series of tests was carried out applying additional imposed bending deformation. The experimental set-up as shown in Fig. 1 was used for this purpose.

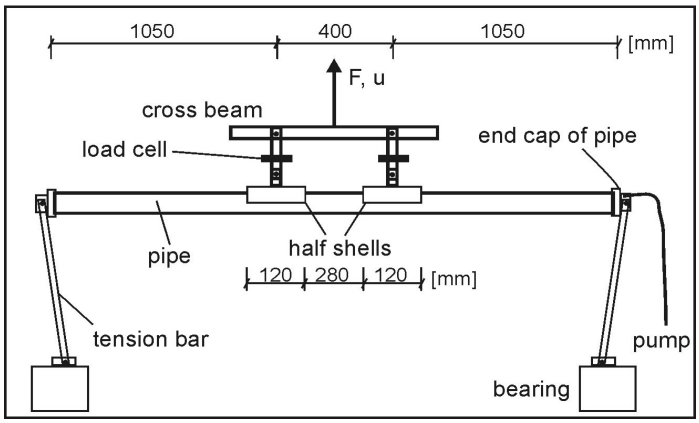

Figure 1: Experimental set-up

This is basically a classical four-point bending test. In order to avoid local failure at the point of load application, a construction with steel half-shells was chosen. The shells were glued to the tension side of the test pipes using a two-pack epoxy resin adhesive. The test specimen is deformed in an upward direction. The points of load application are located at the tension side of the cross-section. The ends of the pipes were simply supported. This experimental set-up proved to be very well suited for the problem under investigation.

Test pipes with an outer diameter of D = 66.1 mm and a nominal wall thickness of t = 0.5 mm (measured average wall thickness 0.54 mm) were used. The pipes consist of steel welded with a longitudinal seam having a yield strength of $f_{y,k}$ = 220 N/mm² and a tensile strength of $f_{u,k}$ = 300 N/mm². The engineering stress-strain-curve was determined by tensile tests on material taken from the coil. The true stress-strain-curve was derived from the engineering stress-strain-curve (see Fig. 2).

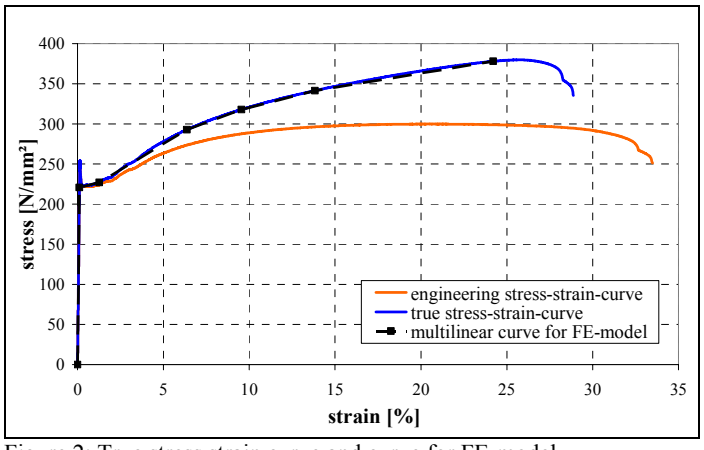

Figure 2: True stress strain curve and curve for FE-model

The test pipes were produced and sponsored by a German company for pipe-systems. The origin of the pipes is a coil of coldformed steel with material number 1.0338 (EN 10027-2). Although the ratio D/t = 132 of these test pipes is not common for onshore pipelines the bearing behavior in elasto-plastic range and the effects of local buckling can also be observed for this thin walled pipe.

Table 1: Test Program

No.	Internal Pressure P [bar]	Imposed Deflection u_k [mm]	Comment
1	0	35.0	
2	15	76.0	
3	15	67.5	Pressure drop to P = 0 and rebuild-up to P = 15 bar
4	25	112.0	
5	25	110.0	Pressure drop to P = 0 and rebuild-up to P = 25 bar
6	5	43.0	
7	30	130.0	
8	30	182.0	Pressure drop to P = 0 and rebuild-up to P = 30 bar

First of all two tests were carried out to calibrate the test equipment and to determine the ideal spacing for the points of load application. The subsequent test series was then undertaken using a distance of 400 mm between the points of load application (see Fig. 1). Maximum stress is expected in the centre of the pipe. The distance of the points of load application is greater than 4D, so that local effects may have died out. Table 1 gives an overview over the test program.

The strains were evaluated using strain gauges attached to the test specimens. The internal pressure and the deformation of the test specimens were recorded online by pressure sensors, inductive direction sensors and potentiometers. The reaction force due to the imposed deflection was measured with two load cells. The internal pressure was applied via filling the pipes with water using a hand-operated pump. No leaks occurred in any of the tests carried out with partly marked local deformations and strains.

NUMERICAL SOLUTION VERSUS TEST RESULTS

The ovalisiation of the pipes 01 to 08 was measured prior to tests because this kind of imperfection has a large influence on the bearing behavior of steel pipes. A measure for the ovalisation is the unroundness which was calculated using the formula

$$f_o = \frac{D_{max} - D_{min}}{D} \qquad (1)$$

This was on average f_o = 2.0 %. The tests were carried out displacement-controlled, whereby pipe 1 was only subjected to bending and pipes 2 to 8 were subjected to bending and internal pressure. The horizontal and vertical deformations were measured using direction sensors and potentiometers. At both points of load application (see Fig. 1) load cells were located to measure the reaction forces due to imposed deflection. In addition strain gauges were installed longitudinal and transverse to the pipes as well as a pressure gauge at one end cap of the pipe.

Fig. 3 shows the curve of average reaction force as a function of the vertical imposed deflection for pipe 1 (P = 0 bar). These parameters were chosen for the comparison with numerical solutions because the values of F and u were directly measured during the test. The average reaction force is the average of the values from the two load cells. The deflection u was measured in the middle of the pipe length.

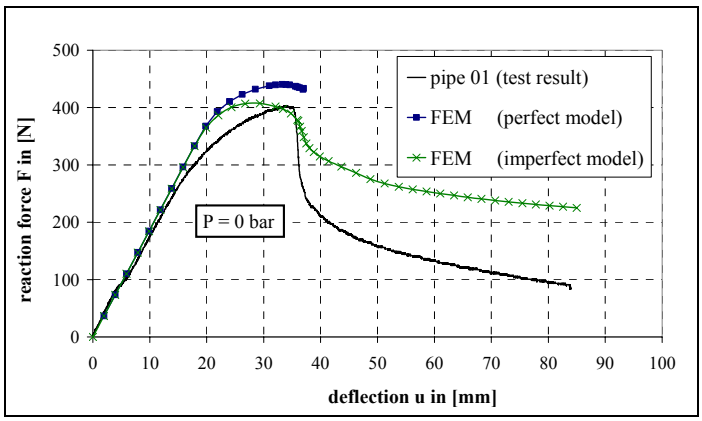

Figure 3: Force-Deflection curves for pipe 1

There is a linear rise in the reaction force at the beginning of the test until the elastic yield strength is reached. The transition to the elasto-plastic range can be recognized at a deflection of approx. u = 16 mm by the non-linear curve progression. A reason for the difference between measured values and calculated values above F = 300 N could be residual stresses due to the production processes (welding, cold forming). These residual stresses are not considered in FE-models. In the event of a further increase in the imposed deflection shell buckling is initiated by existing geometrical and material imperfections. After the onset of local buckling has occurred, the global deflection u will continue, but more and more energy of the applied bending energy will be accumulated in the local buckle. Shortly after reaching the maximum moment bearing capacity (u = 35 mm, F = 400 N) a geometrical collapse occurs, whereby the buckle springs inwards near midspan of the pipe. At the same time there is a significant drop in the force-deflection curve whereby a distinct reduction in the moment bearing capacity occurs.

Numerical simulations were made using the FE-program ANSYS for comparison with the test results. The model was generated with shell elements using symmetrical conditions. The true stress-strain curve of the tensile tests was implemented as material law (see Fig. 2).

The FE-calculations show a good agreement for the curves in the elastic range. The calculation with the perfect model achieves a maximum force of F = 440 N and ends with a deflection of u = 37 mm. For the calculation with imperfections, first of all the buckling mode has to be selected, which qualitatively shows the deformation pattern of the test. This is done by an eigenvalue analysis. Quantitative values of the imperfections in the area of the chosen buckling mode are based on the measured values of ovalisation (unroundness f_o). The force-deflection curve of the model with imperfection has at u = 27 mm a maximum force of F = 407 N, which declines at u = 35 mm. Contrary to the model with perfect pipe this force-deflection curve extends right into the softening region, but the decline in force, however, can not be seen so clearly in comparison to test pipe 1.

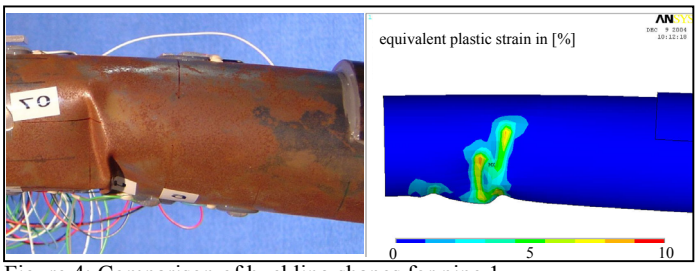

Figure 4: Comparison of buckling shapes for pipe 1

The buckle shapes of test pipe 1 and of the FE-calculation with imperfect model are compared in Fig. 4. The start of buckling was located on the compression side near midspan of the pipe. Position and form of the buckles show a good agreement.

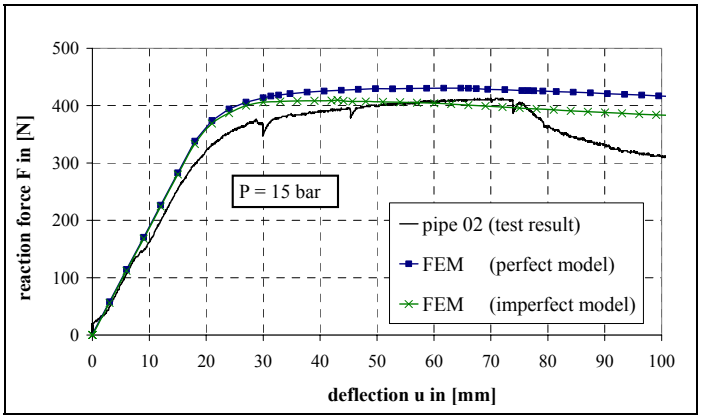

Figure 5: Force-Deflection curves for pipe 2

In case of pipe 2 an internal pressure of P = 15 bar was applied via filling the pipe with water using a hand-operated pump. The ratio of the hoop stress to the yield strength was $\sigma_\Theta / \sigma_y = 0.45$. Subsequently the imposed deflection was increased, whereas the internal pressure was kept constant. At u = 45 mm, where pipe 1 already showed failure due to local buckling, the imposed deflection was stopped, to undertake a visual inspection. No buckling or wrinkling of the pipe was discovered. Only at approx. u = 60 mm several ripples could be recognized along the pipe axis on the compression side. At u = 76 mm the deformation of a single ripple (wave) increased and a buckle became more significant, and bulged outwards due to the stabilization caused by internal pressure. At the same time a decrease for the reaction force could be observed at the load cells.

The numerical simulation without imperfections reaches a maximum value of F = 430 N for the reaction force at u = 62 mm (see Fig. 5). In the case of the calculation with the imperfect model the maximum value is F = 407 N. Contrary to the test result, both numerical force-deflection curves show no significant drop in force where the single buckle occurred in the test. In comparison to pipe 1 greater deflections could be achieved without stability failure both in the test as well as in the simulation due to the increased buckling resistance caused by the internal pressure.

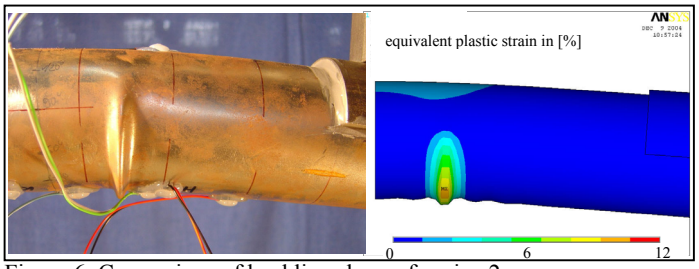

Figure 6: Comparison of buckling shapes for pipe 2

The buckling shapes of test pipe 2 and the FE-calculation with the imperfect model are compared in Fig. 6. The start of buckling took place on the compression side near midspan of the pipe. Position and form of the buckles can be seen to correspond very well. The wrinkles that are built up along the pipe axis in the prebuckling phase are also visible in the FE-simulation. In comparison to the test without internal pressure (pipe 1) the buckling behavior in the case of tests with internal

pressure (pipes 2 to 8) is fundamentally different, because the hoop stresses due to internal pressure counteract the ovalising forces due to bending and so the buckling occurs for greater imposed deformations. The buckling figures under internal pressure are characterized by the establishment of a single buckle which develops outwards in a relatively narrow area with regard to the longitudinal direction of the pipe. The smoothing effect of the internal pressure on the imperfection leads to a further stabilisation of the tubular steel.

In the case of pipe 3 a pressure drop scenario was investigated in the elasto-plastic range. At first the pipe was deformed under an internal pressure of P = 15 bar up to a vertical deflection of u = 49 mm. After that the pipe was unloaded from P = 15 to 1 bar, while the imposed deformation was kept constant. The pipe cross-section remained stable thereby and no local buckling occurred. Only the reaction forces dropped back to the load level in relation to the actual static yield limit. After renewed pressure build-up to P = 15 bar the imposed deformation was increased further. At u = 67.5 mm the internal pressure was again reduced to 1 bar for the second time, whereby the pipe still remained stable and no buckling occurred. Only when the deflection u was further increased without pressure buckling failure immediately occurred in the compression zone. The form of buckling resembled that of the pipe 1 without internal pressure.

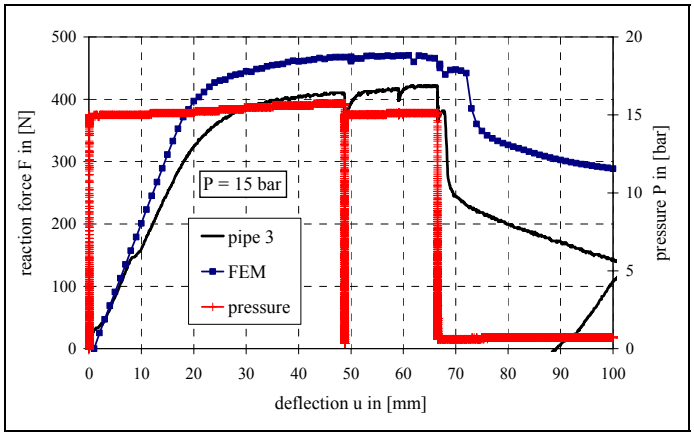

Figure 7: Force-Deflection curves for pipe 3 with pressure drop

This elasto-plastic bearing behavior could be confirmed with an FE-calculation, where a pressure drop at u = 49 mm and u = 67.5 mm was simulated. In the case of both stop positions the pipe remained stable. Only in the case of a further increase without internal pressure a sudden buckle failure occurred similar to that in the case of the tested pipe 3. It was possible to repeat this phenomenon using the tests with the pipes 5 and 8 for different internal pressures. That means, for a phase, where the deformation is kept constant, the internal pressure is not necessary for the stability of the pipe. But a further increase of deformations must not occur in unpressurized condition, because the supportive effect of the internal pressure during development of further plastic strain increments is missing.

Furthermore, a gradual pressure reduction due to the increase in the volume of the pipes could be observed in the elasto-plastic range. This led to a gradual increase in the reaction forces, because assuming the Mises flow-hypothesis and a biaxial stress state a greater longitudinal stress (bending) due to the drop in the hoop stress (internal pressure) could be allowed considering the actual equivalent stress (see Eq. 2).

$$\sigma_V = \sqrt{\sigma_L^{\,2} + \sigma_\Theta^{\,2} - \sigma_L \cdot \sigma_\Theta} \qquad (2)$$

STRAIN-LIMITS OF MODEL-SCALE TESTS

A limit criterion based on the consideration of plastic strains is needed for the following analytical method. Fig. 8 shows the critical strains of the tested pipes as a function of the internal pressure. The values for ε_{cr} originate from the strain gauges on the compression side for the longitudinal direction (axial direction) at the beginning of buckling. A good approximation to the experimental limit strain curve is provided by equation 4. But for a limit criterion in the analytical method the empirical equation 3 is used because the values calculated with equation 3 are more on the safety side for higher pressure ratios.

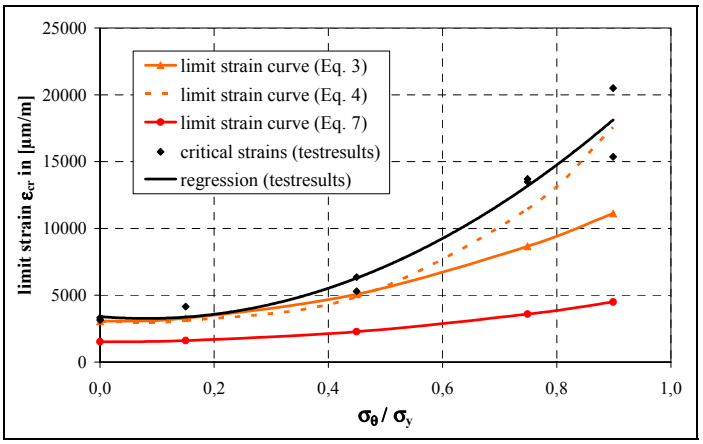

Figure 8: Critical compressive strain limits for plastic buckling

Table 2: Test results

Test No.	Internal Pressure P [bar]	Pressure ratio σ_θ / σ_y [-]	Critical compressive strain ε_{cr} [µm/m]
1	0	0.00	3320
2	15	0.45	5300
3	15	0.45	6350
4	25	0.75	13500
5	25	0.75	13700
6	5	0.15	4160
7	30	0.90	15360
8	30	0.90	20500

for $r_m/t = 65.6$: $$\varepsilon_{cr} = 0.2 \cdot \frac{t}{r_m} + 0.01 \cdot \left(\frac{\sigma_\Theta}{\sigma_y}\right)^2 \qquad (3)$$

$$\varepsilon_{cr} = 0.2 \cdot \frac{t}{r_m} + 0.02 \cdot \left(\frac{\sigma_\Theta}{\sigma_y}\right)^3 \qquad (4)$$

The first term of Eqs. 3 and 4 applies for the case of pure bending. The second term takes into consideration the increased buckling resistance due to internal pressure depending on the ratio of hoop stress to elastic yield strength. In literature (Reddy 1979 and Bai 2003) for plastic shell buckling at pure bending a range for the critical buckling strains of

$$0.2 \cdot \frac{t}{r_m} < \varepsilon_{cr} < 0.4 \cdot \frac{t}{r_m} \qquad (5)$$

is given. The increased buckling resistance due to internal pressure is taken into consideration according to a suggestion of Gresnigt (1986) in semi-empirical equations (Eqs. 6 and 7). Based on test results values for buckling strains are indicated as dependent on pipe slenderness, Young's-modulus and internal pressure.

$$\text{If } \frac{t}{r'} > \frac{1}{60}: \quad \varepsilon_{cr} = 0.25 \cdot \frac{t}{r'} - 0.0025 + 3000 \cdot \left(\frac{P \cdot r}{E \cdot t}\right)^2 \cdot \frac{|P|}{P} \tag{6}$$

$$\text{If } \frac{t}{r'} \le \frac{1}{60}: \quad \varepsilon_{cr} = 0.1 \cdot \frac{t}{r'} + 3000 \cdot \left(\frac{P \cdot r}{E \cdot t}\right)^2 \cdot \frac{|P|}{P} \tag{7}$$

$$\text{with } r' = \frac{r}{1 - \frac{3a}{r}} \tag{8}$$

In comparison to the equations 3 and 4 Gresnigt already gives design values and takes the ovalisation into account (Eq. 8).

ANALYTICAL SOLUTION VERSUS TEST RESULTS

The analytical method is based on differential equations (D.E.) for beams. The static system and loading conditions of the test pipes are shown in Figure 9. It is to be noted that a longitudinal tensile force N is produced by the internal pressure on the pipe end caps. Because of that the general differential equation for beams with longitudinal tensile force (Eq. 9) is used for the analytical solution.

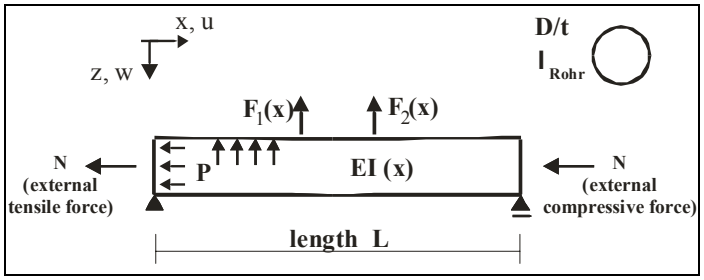

Figure 9: Static system of model-scale tests with loading

$$\left(EI \cdot w''(x)\right)'' + N \cdot w''(x) = F(x) \tag{9}$$

The solutions of the differential equation for w(x), ϕ(x), M(x) and Q(x) are calculated with trigonometrical constitutive functions as series expansions. No external forces N are applied (N = 0) in the test specimen. If N ≠ 0 a case differentiation is to be made. Furthermore, the bending stiffness is not constant in the elasto-plastic range, so that the general D.E. is used with EI(x). For the consideration of greater deformations the exact differential geometrical relationship between the deflection w(x) and the curvature κ(x) is implemented:

$$\kappa(x) = \frac{w''(x)}{\left(1 + w'(x)^2\right)^{3/2}} \tag{10}$$

The analytical method is subdivided into an elastic and elasto-plastic part. The elasto-plastic calculation is carried out displacement-controlled and as an iterative method to determine the solutions for w(x), ϕ(x), M(x) and Q(x). The yield criterion according to v. Mises and the material law according to Prandtl-Reuss are selected to consider the plasticity. The total axial strain is then the sum of the elastic strain and the plastic strain increments:

$$\varepsilon_{tot}(x) = \varepsilon_{el}(x) + \sum_{i=1}^{n} \varepsilon_{pl,i}(x) \tag{11}$$

In each iteration-step the borders between elastic and plastic region are newly calculated along the pipe axis (x-direction). In the elasto-plastic range the reduction of the bending stiffness EI(x) depending on the strain values on the tensile side max ε_Z and compression side max ε_D takes place. For this purpose the integral of the inner bending moment to the actual strain condition is calculated on the maximum stressed pipe cross-section.

$$\begin{aligned} M(x) &= 2 \cdot t \cdot r^2 \cdot \int \sigma_t(\max\ \varepsilon_t) \cdot \sin\theta \cdot d\theta \\ &+ 2 \cdot t \cdot r^2 \cdot \int \sigma_c(\max\ \varepsilon_c) \cdot \sin\theta \cdot d\theta \end{aligned} \tag{12}$$

Since the true stress-strain curve is implemented in the analytical method, the true stresses at each strain condition are determined ($\sigma_t = f(\max\ \varepsilon_t)$ and $\sigma_c = f(\max\ \varepsilon_c)$). As a consequence of this no simplifying assumptions (e.g. ideal-elastic, ideal-plastic) had to be implemented in the material law.

To compare the numerical solutions with the test results for the axial strain always the values for L/2 of the pipe were used. The axial strain curves for the compression side at the midspan point of the pipe are compared in Figure 10. There is a very good agreement up to the elastic strain limit for the strain curve of pipe 1 with the numerically and analytically calculated strain curves. At approx. $\varepsilon_{cr} = 3250$ µm/m plastic shell buckling occurs on pipe 1 and after this the axial strain decreases (postbuckling range) because the strain gauges were not located at the local buckle. In the area of the local buckle strains will be much higher. FE-calculation with the perfect model shows very high strain values because the strain was taken from a point at midspan of the pipe where the local buckle occured.

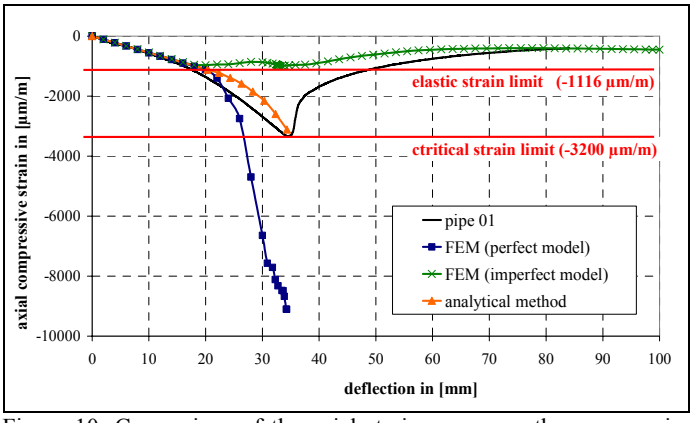

Figure 10: Comparison of the axial strain curves on the compression side

The strain curve of the FE-calculation with imperfect model remains below the elastic strain limit. Using the analytical method according to Eq. 3 a critical strain value of $\varepsilon_{cr} = 3050$ µm/m is established. Furthermore it can be seen that applying the analytical method the nonlinear increase in the axial strain is determined within the elasto-plastic range.

In order to take the biaxial stress status due to bending and internal pressure and assuming von Mises yield criterion (see Eq. 2) the following equation is derived (shear stresses will be negligible):

$$0 = \sigma_L^2 - \sigma_L \sigma_\Theta + \sigma_\Theta^2 - \sigma_v^2 \tag{13}$$

This quadratic equation has two solutions for σ_L, if hoop stress σ_Θ and the equivalent stress σ_v (limit stress for v. Mises criterion) are known:

$$\sigma_{L1;L2} = \frac{\sigma_\Theta}{2} \pm \sqrt{\sigma_v^2 - 0.75 \cdot \sigma_\Theta^2} \tag{14}$$

Furthermore, σ_t for tensile zone and σ_c for compressive zone of the pipe are formulated for the solutions of longitudinal stress σ_L as a function of the hoop stress σ_Θ and the equivalent stress σ_v:

$$\sigma_{t;c} = \frac{\sigma_\Theta}{2} \pm \sigma_v \cdot \sqrt{1 - 0.75 \cdot \left(\frac{\sigma_\Theta}{\sigma_v}\right)^2} \tag{15}$$

To determine the maximum elastic strain increments in axial direction for the bending at the limit criterion by v. Mises, the elastic strain increments of external axial force N (N = positive for tensile force), axial strain as a result of cap pressure and traverse strain due to internal pressure are considered:

$$\varepsilon_{b,t} = \frac{\sigma_t}{E} - \frac{N}{EA} - \frac{P \cdot D}{4 \cdot t \cdot E} + \nu_{el} \cdot \frac{P \cdot D}{2 \cdot t \cdot E} \tag{16}$$

The value $\varepsilon_{b,t}$ is the maximum bending strain on the tensile side of the pipe which can be provided within the elastic range ($\varepsilon_{b,c}$ analog with Eq. 16 but with opposite sign).

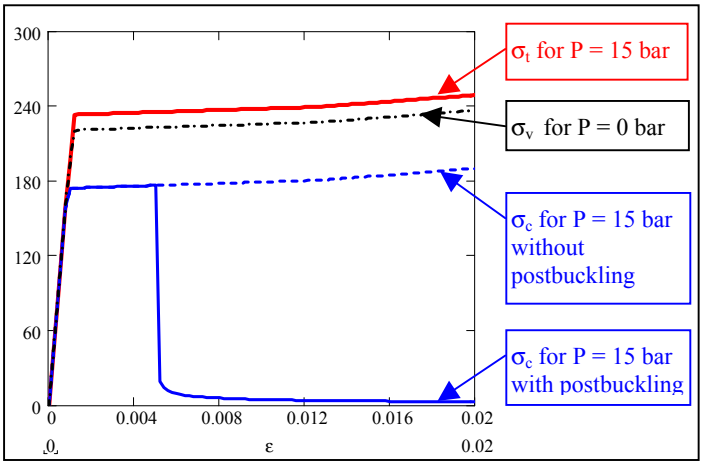

Figure 11: Stress-strain-curves for tensile and compressive range

The stress-strain curves of the tensile- and compressive side are identical for P = 0 bar. If P ≠ 0 bar, then according to the Mises yield criterion different values are determined for the maximum longitudinal stress in the tension- and compression zone of the pipe (see Eq. 15).

The postbuckling behavior within the compression zone is approximated by an empirical formula. It was derived with curve fitting for the tests carried out in this program. It has to be checked for other D/t ratio's.

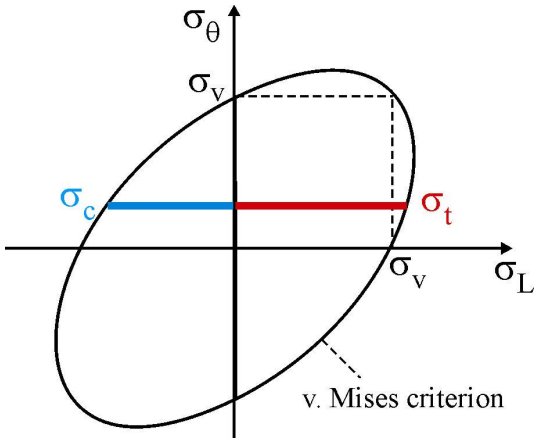

Figure 12: v. Mises ellipse for biaxial stress status

The drop in stress for the compressive side is described depending on the ratio σ_Θ / σ_y and the critical strain value ε_{cr}. Because of this a simulated decrease in the reaction force occurs concerning the force-deflection curve. If the hoop stress is high, the reaction force will slightly drop within the postbuckling range. But if the hoop stress is low or zero, the reaction force decreases more distinct within the postbuckling range.

$$\text{postbuckling}(\varepsilon) = \frac{\sigma_c}{1 + 400 \cdot (\varepsilon - \varepsilon_{cr})^{\frac{\sigma_\Theta}{\sigma_v}}} \qquad \text{for } (\varepsilon > \varepsilon_{cr}) \tag{17}$$

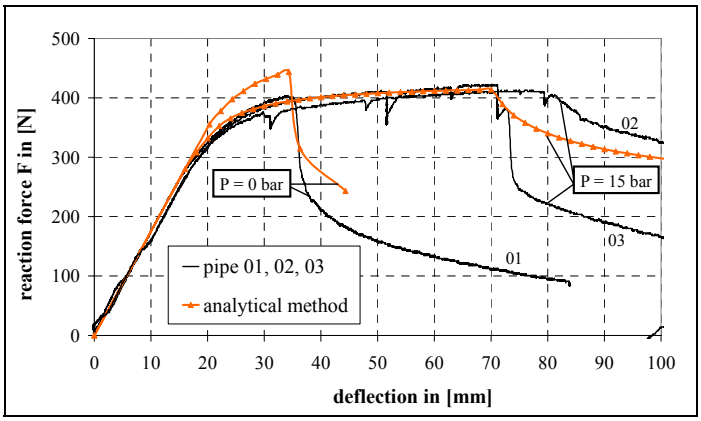

Figure 13: Comparison of the analytical calculation with the tests

The results of the analytical method and of the tests with P = 0 und 15 bar are compared in Figure 13. In the case of the analytical calculations the strain-based limit criterion according to Eq. 3 is applied. For the case without internal pressure (pipe 1) a significant drop occurs after the critical strain has been reached on the compressive side. The force-deflection curve of pipe 1 does not reach the maximum value of the analytical method, because the influence of material and geometrical imperfections is not taken into account by the analytical method. The imperfections decrease the load bearing capacity significantly in the unpressurized condition, so the force-deflection curve of pipe 1 is rather nonlinear.

In the case where P = 15 bar greater deflection and greater axial strains are reached before plastic shell buckling occurs. The region of

postbuckling is reached with a slightly lower deflection in the analytical calculation, because according to Eq. 3 the value for the limit strain ε_{cr} at $\sigma_\Theta / \sigma_y = 0.45$ lies below both test values and is therefore on the safer side. The drop in the reaction force of pipe 2 (P = 15 bar) and analytical calculation is smoother than in the case of pipe 1 (P = 0 bar) due to the stabilizing effect of internal pressure. The decrease in reaction force of pipe 3 is more distinct than in the case of pipe 2, because for pipe 3 the scenario of a pressure reduction in the elasto-plastic range was investigated, and from u = 67.5 mm it was further deformed pressureless. For this reason the buckle failure of pipe 3 after approx. u = 70 mm resembles rather the test without internal pressure (pipe 1), characterized by a steep decline in force. The curves of pipe 2 and 3 show a better conformance with the analytical calculation in the prebuckling phase than the comparison for pipe 1, because the internal pressure causes a smoothing of the imperfections and thus the load-bearing capacity is not so markedly reduced. This elasto-plastic bearing behavior under internal pressure and imposed deformation could be verified by further tests (4 – 8) with a variation of internal pressure.

TRANSFER TO REAL BOUNDARY CONDITIONS

The experimental set-up for the test specimen is a closed system. An axial tensile stress acts at the pipe end caps resulting from internal pressure. The test specimen can be freely deformed in horizontal direction due to the boundary conditions at the pipe ends and thus follow a longitudinal change caused by bending without hindrance. The boundary conditions of a buried pipeline do not correspond with these test boundary conditions. A buried pipeline has basically no end caps and therefore also no longitudinal stresses resulting from internal pressure. Deflection forces associated with change in direction within bends of pipes are countered due to the embedding in the soil via friction over a short interval. Solely from the transverse contraction of the pipeline a resultant stress occurs in axial direction, which in the case of the material steel is equivalent to 30 % of the hoop stress caused by internal pressure.

The ends of the test specimens are horizontally non-braced. This means that the axial displacement of the test specimen resulting from the upthrust curvature can occur without hindrance. This is not possible in the case of a buried pipeline. It can be assumed that the pipeline is laid straight and cannot shift in order to give way to a strain as a result of bending until static friction is overcome.

This has a supporting influence on the pipe sections in settlement areas because axial soil friction forces stiffen the pipeline and therefore limit the curvature and moment in those areas.

It has to be remarked, that pipelines under thermal loading will behave different. Under sub-zero conditions, the soil surrounding the pipe freezes and soil friction will be reduced to almost zero. High temperature pipelines, which are anchored due to soil friction will be subjected to axial compression which may be lead to increasing curvature in settlement areas.

CONCLUSION

Experimental and numerical investigations from an ongoing research project are presented about steel pipes subjected to combined loading from internal pressure and bending.

The investigations have shown that as far as the problem of “Bending of a pipeline under internal pressure” is concerned this is not mainly a question of bending strength but rather a problem of deformation capacity (e.g. buckling). The internal pressure has a supporting effect which significantly reduces the pipe’s susceptibility to buckling.

A good agreement between test results and numerical simulation was achieved. Even highly concentrated nonlinear states such as buckling patterns and various load histories were simulated correctly. Parallel to the numerical simulation it was possible to reproduce the bearing-behavior within the elasto-plastic range analytically adopting differential relationships. Based on these investigations it was possible to formulate a general approach to the indication of critical limit strains. The problem of transfering the test results to real boundary conditions was discussed.

It was the aim to formulate generally valid principles. For this reason the investigations were carried out on the basis of characteristic values and safety coefficients are not included. These are to be adapted to meet the national guidelines and applications for real design problems.

ACKNOWLEDGEMENT

The authors thank the German Federation of Industrial Cooperative Research Associations "Otto von Guericke" (AiF) for funding the research work within the program “Future Technologies for Small and Medium Companies” (ZUTECH).

REFERENCES

ASME (1998). “Boiler and Pressure Vessel Code (BPVC)”, *ASME,* Pt III

Bai, Y. (2003). “Marine structural design” *Elsevier,* Amsterdam

DIN EN 1594 (2000). “Gas supply systems – Pipelines for maximum operating pressure over 16 bar – Functional requirements” Ref.-Nr. DIN EN 1594:2000-09

Galambos, T. V. (1998). “Guide to stability design criteria for metal structures”, *John Wiley & Sons,* 5th edition

Gresnigt, A. M. (1986). “Plastic design of buried steel pipelines in settlement areas”, *Heron,* Vol. 31 No. 4

Hauch, S. and Bai, Y. (1999). “Bending Moment Capacity of Pipes”, *Proceedings of the 18th International Conference on Offshore Mechanics and Arctic Engineering,* OMAE, St Johns, Newfoundland Canada Paper No PL-99-5033

Krysik, R. (1994). “Stability of steel truncated cone and cylindrical shells under axial compression and internal pressure”, *“Stabilität stählerner Kegelstumpf- und Kreiszylinderschalen unter Axial- und Innendruck”*, *Dissertation* University of Essen, Germany

Reddy, B. D. (1979). “An Experimental Study of the Plastic Buckling of Circular Cylinder in Pure Bending”, *Int. J. Solid and Structures,* Vol. 15, pp. 669-683

Zimmerman, T. J. E. and Stephens, M. J. and De Geer, D. D. and Chen, Q. (1995). “Compressive strain limit for buried pipelines”, *Proceedings of the 14th International Conference on Offshore Mechanics and Arctic Engineering,* OMAE, Copenhagen, Vol. V - Pipeline Technology